Structural Engineering and Mechanics, *Vol. 47, No. 3 (2013) 331-343*
DOI: http://dx.doi.org/10.12989/sem.2013.47.3.331

Sloshing characteristics of an annular cylindrical tuned liquid damper for spar-type floating offshore wind turbine

S.H. Jeon, M.W. Seo, Y.U. Cho, W.G. Park and W.B. Jeong*

School of Mechanical Engineering, Pusan National University, Busan 609-735, Korea

(Received August 6, 2012, Revised July 14, 2013, Accepted July 17, 2013)

Abstract. The natural sloshing frequencies of annular cylindrical TLD are parametrically investigated by experiment, aiming at the exploration of its successful use for suppressing the structural vibration of spar-type floating wind turbine subject to multidirectional wind, wave and current excitations. Five prototypes of annular cylindrical TLD are defined according to the inner and outer radii of acryl container, and eight different liquid fill heights are experimented for each TLD prototype. The apparent masses near the first and second natural sloshing frequencies are parametrically investigated by measuring the apparent mass of interior liquid sloshing to the acceleration excitation. It is observed from the parametric experiments that the first natural sloshing frequency shows the remarkable change with respect to the liquid fill height for each TLD model with different container dimensions. On the other hand, the second natural sloshing frequency is not sensitive to the liquid fill height but to the gap size, for all the TLD models, convincing that the annular cylindrical sloshing damper can effectively suppress the wave- and wind-induced tilting motion of the spar-type floating wind turbine.

Keywords: annular cylindrical sloshing damper; spar-type floating offshore wind turbine; multi-directional and varying-frequency; tilting motion; natural sloshing frequency; apparent mass

1. Introduction

As a representative renewable energy generation mechanism, wind turbines were initially designed for the ground installation and showed the rapid increase in both the total installation number and the maximum power generation capacity (Hansen and Hansen 2007). However, this rapid increase encountered several obstacles such as the infringement of living environment, the limitation of being high-capacity and making large wind farm. This critical situation naturally turned the attention to the offshore sites, a less restrictive installation place. Offshore wind turbines are classified largely into two categories, fixed- and floating-type according to how the wind turbine tower is supported. Differing from the fixed-type, the floating-type wind turbine is under the concept design stage because several core technologies are not fully settled down (Karimirad *et al*. 2011), particularly the maintenance of structural dynamic stability against irregular external excitations (Faltinsen 1990).

The structural dynamic stability of floating-type wind turbine is greatly influenced by wind, wave and current, and it is quantitatively evaluated in terms of three rigid body translation motions

*Corresponding author, Professor, E-mail: wbjeong@pusan.ac.kr

http://www.techno-press.org/?journal=sem&subpage=8 ISSN: 1225-4568 (Print), 1598-6217 (Online)

(i.e., surge, sway and heave) and three rigid body rotations (i.e., pitch, roll and yaw) (Cho *et al*. 2012). Among them, roll and pitch motions are mostly considered because these two rigid body rotations give rise to the crucial impact on the tilting of floating-type wind turbine. The tilting motion may not only degrade the power generation efficiency, but it may capsize the entire wind turbine in worst case. Floating-type wind turbines are positioned and stabilized, to some extent, by a combination of body weight, buoyancy force, mooring cables or tension legs, but such a basic control is insufficient to suppress the tilting motion caused by severe aero- and hydro-excitations. In this connection, the need of more effective damping devices has been increased, and the application of traditional tuned liquid damper (TLD) and tuned liquid column damper (TLCD) to floating-type wind turbines are intensively studied (Lee *et al*. 2006, Jin *et al*. 2007, Colwell and Basu 2009).

TLD and TLCD were originally introduced to suppress the structural vibration of high-rise buildings subject to earthquake and wind loads (Miyata *et al*. 1989, Balendra *et al*. 1995, Yamamoto and Kawahara 1999). As is well known, these passive dampers utilizing the interior liquid sloshing (or, liquid fluctuation) can alter the free vibration characteristic of high-rise buildings by means of the interior liquid sloshing (or, liquid fluctuation), in order to avoid the resonance phenomenon to the external excitation. One prominent feature of TLD and TLCD is that their first sloshing frequency can be controlled by adjusting the liquid fill height and the geometric dimensions of horizontal and vertical tubes. Balendra *et al*. (1995) reported that the damping performance of TLCD is better than TLD, but its damping performance is dependent of the direction of excitation. Meanwhile, the geometry of TLD is not suitable to install it into the cylindrical tower of wind turbine. Therefore, a TLD which is excitation direction-independent and easily installed is highly desired.

In this context, the goal of the current study is to experimentally explore the possibility of annular cylindrical sloshing damper as an effective damping device for spar-type floating wind turbine. The annular cylindrical sloshing damper is not only excitation direction-independent, but it can be easily installed by simply fitting it into the outer surface of cylindrical tower. But, it has been reported that the circular TLDs exhibit the remarkable nonlinear variation of the fundamental natural sloshing frequency to the liquid fill height and geometric dimensions of TLD owing to the free surface breaking of interior liquid (Morsy 2010). In this paper, the fundamental natural sloshing frequency is parametrically investigated with respect to various combinations of the liquid fill height, inner and outer radii of TLD.

2. Dynamic response stabilization of floating wind turbine

2.1 Rigid dynamic response of spar-type floating wind turbine

A typical spar-type floating offshore wind turbine is represented in Fig. 1(a), where tower and floating platform is divided roughly by the sea water free surface. The vertical position of floating wind turbine is determined by the balance of the total weight of wind turbine, buoyancy force and tension of mooring cables. The upper part composed of wind blades, nacelle and tower is subject to wind load, while the lower floating platform is under wave- and current-induced hydrodynamic pressure as well as the tension of mooring cables. The spar-type floating wind turbine is usually moored at offshore by three equal mooring cables which are anchored at the seabed. The reader may refer to Lefebvre and Collu (2012) for more details on the roles of wind turbine components

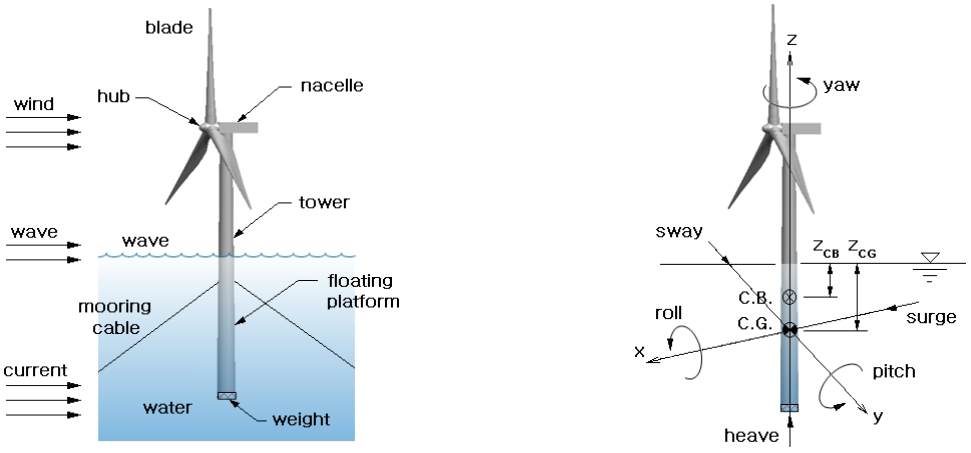

Fig. 1 Representation: (a) spar-type floating wind turbine, (b) rigid body motion with 6 DOFs

and the design issues of floating wind turbine.

Referring to Fig. 1(b), the rigid body motion $\boldsymbol{R} \in \Re^3$ at a position $\boldsymbol{r}$ within offshore wind turbine is decomposed into the rigid translation $\boldsymbol{s} \in \Re^3$ and the rigid rotation $\boldsymbol{\Omega} \in \Re^3$ such that

$$\boldsymbol{R} = \boldsymbol{s} \oplus \boldsymbol{r} \times \boldsymbol{\Omega} \tag{1}$$

$$\boldsymbol{s} = \eta_1 \boldsymbol{i} + \eta_2 \boldsymbol{j} + \eta_3 \boldsymbol{k}\ , \quad \boldsymbol{\Omega} = \eta_4 \boldsymbol{i} + \eta_5 \boldsymbol{j} + \eta_6 \boldsymbol{k} \tag{2}$$

In which η_1, η_2 and η_3 denote surge, sway and heave motions, while η_4, η_5 and η_6 indicate roll, pitch and yaw motions, respectively. Introducing the (6×6) wave and viscous damping matrices $\boldsymbol{B}$ and $\boldsymbol{b}$, the added mass (or, moment of inertia) matrix $\boldsymbol{A}$ and the restoring stiffness matrix $\boldsymbol{C}$, the generalized coupled rigid body motions can be expressed by (Biran 2003, Cho *et al*. 2012)

$$(\boldsymbol{M} + \boldsymbol{A})\ddot{\eta} + (\boldsymbol{B} + \boldsymbol{b}\delta_{4j})\dot{\eta} + \boldsymbol{C}\eta = Re(\boldsymbol{F}e^{i\omega_E t}) \tag{3}$$

In which, $\boldsymbol{M}$ and $Re(\boldsymbol{F}^{-i\omega_E t})\, F_i^w$ denote the mass matrix of offshore wind turbine (or, moment of inertia) and the vector of sinusoidal exciting force and moment.

Among six components of rigid body motion, the tilting of floating wind turbine is directly related to the roll and pitch motions. As mentioned earlier, the tilting motion may not only decrease the power generation efficiency, but it may capsize the entire wind turbine in worst case. Pitch and roll motions which are caused by the action of wind, wave and current loads are controllable by the center of gravity (CG), center of buoyancy (CB) and the position of mooring which are caused by the action of wind, wave and current loads cables. It has been found, from the theoretical work by Karimirad *et al*. (2011), that the pitch/roll stiffness increases as the centers of gravity and buoyancy become lower and higher respectively. In other words, the natural pitch/roll frequencies increases in proportional to the relative distance between CB and CG. The location of mooring cables, which is in the correlation with CB and CG, affects the cable tension and the dynamic stability of floating wind turbine. The tilting motion of floating wind turbine could be

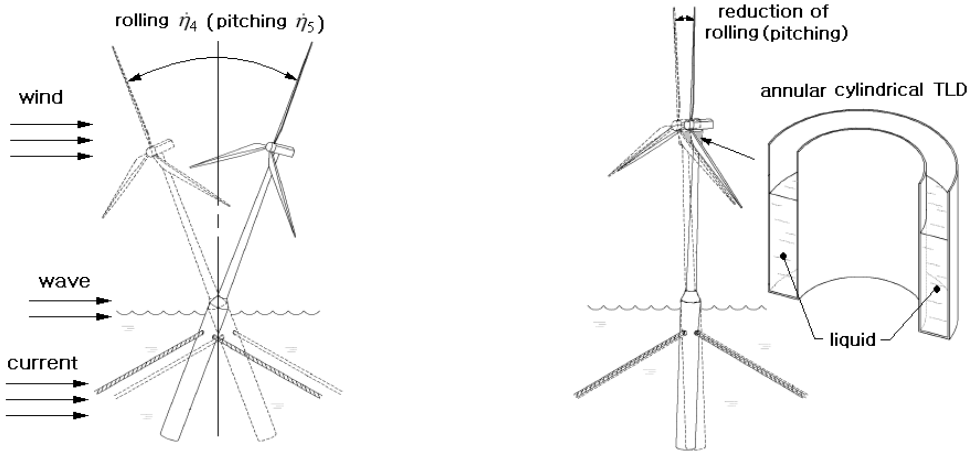

Fig. 2 Rigid body motion of offshore wind turbine: (a) without TLD, (b) with TLD

reduced to some extent if these three locations were appropriately chosen, but an effective damping device is desired to aggressively control the tilting motion.

2.2 Annular cylindrical TLD for spar-type floating wind turbine

The tilting motion of spar-type floating wind turbine without extra damping device is schematically represented in Fig. 2(a). Wind turbine blades are subject to wind load so that wind load contributes mostly to pitch motion, while wave and current loads acting on the cylindrical floating platform give rise to both pitch and roll motions. Similar to TLDs installed in high-rise buildings, the annular cylindrical TLD for spar-type floating wind turbine is installed at the top of wind tower as illustrated in Fig. 2(b) in order to maximize the structural damping performance. The inner radius of annular cylindrical TLD is set by the radius of wind tower at the top in order for the fitting assembly.

The fluctuation of liquid free surface called liquid sloshing gives rise to the harmful hydrodynamic impact on the container, and various types of sloshing suppression devices like baffle are installed within liquid containers (Cho and Lee 2002, 2004). On the contrary, liquid sloshing is usefully utilized to absorb the structural vibration energy generated by earthquakes, wind and wave loads. The absorption of vibration energy alters the free vibration behavior of huge tall structures to prevent the resonance phenomenon, which motivated to the introduction of TLD as a passive damping device for huge tall structures subject to various dynamic excitations.

TLDs can be classified into shallow TLD and deep TLD based on the relative liquid fill height to the damper length. According to Dean and Dalrymple (1984), the limit of the relative liquid fill height of shallow TLD is around 10~12%. It has been known that shallow TLDs provide the desired high damping thanks to the wave breaking phenomenon. Wave breaking increases the damping performance such that the damping magnitude of shallow TLD is an order as high as deep TLDs. However, Morsy (2010) reported that shallow TLD is not practical owing to the extreme nonlinearity stemming from the large free surface fluctuation (Cho and Lee 2004) and the occurrence of unpredictable wave breaking. Liquid in shallow TLD exhibits the extreme free

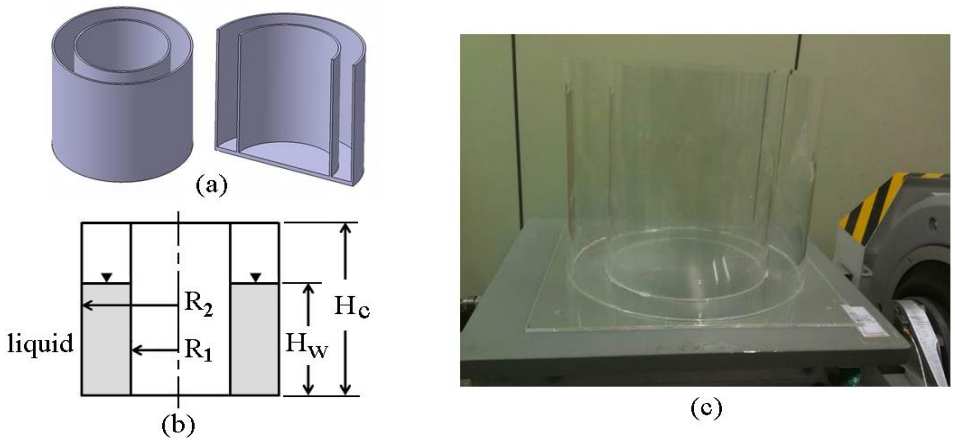

Fig. 3 Annular cylindrical TLD: (a) CAD model, (b) dimensions, (c) acryl prototype

surface fluctuation with the amplitude equal to the liquid fill height, which causes the unpredictable wave braking phenomenon. Owing to the highly nonlinear liquid sloshing including the wave breaking phenomenon, the sloshing frequency tuning of shallow TLD becomes difficult. Meanwhile, all the previous studies have shown that the damping performance of TLD increases in proportional to the total mass of interior liquid, but the increase of total liquid mass is not desirable for floating wind turbine. In this context, the total amount of liquid in the annular cylindrical TLD introduced in this paper is less than usual circular TLDs, for the same liquid fill height. Besides the multi-directional mass-effectiveness, the annular cylindrical TLD with the large liquid fill height does neither cause large free surface fluctuation nor wave breaking.

3. Parametric experiments of apparent mass of annular cylindrical TLD

Fig. 3(a) shows a CAD model of annular cylindrical TLD and the major geometry dimensions are represented in Fig. 3(b). The contained is manufactured with acryl for clear visualization of the free surface fluctuation of liquid and water is used as liquid. Fig. 3(c) shows a small-scale prototype of acryl annular cylindrical TLD, and five prototypes with different radii given in Table 1 are prepared for the parametric experiments of apparent mass. The height H_c of acryl container is set by 300 mm and the liquid fill height H_w is taken variable. The density, Young's modulus and Poisson's ratio of acryl are as follows: E_c = 2.80 Gpa, ν_c = 0.37 and ρ_c = 1,180 kg/m^3 respectively.

In this study, the experiments were repeatedly conducted by eight times for each TLD model for the sake of the reliability of experimental data. Since the difference between R_1 and R_2 is relatively small while the liquid fill height H_w is relatively large with respect to the container height h_c, the annular cylindrical TLDs under consideration belong to a type of deep TLD. Therefore, the nonlinear large liquid fluctuation including wave breaking does not prevail, from which it is expected that the natural sloshing frequencies of the current annular cylindrical TLD will be more easily tuned than usually circular TLDs. In addition, the total amount of liquid filled in the current annular TLD is significantly smaller than usual circular TLD for the same relative liquid fill height so that the hydrodynamic impact on the container and structural system can be minimized.

Table 1 Inner and outer radii of annular cylindrical TLD models

Models	A	B	C	D	E
R_1 (mm)	80	100	120	145	145
R_2 (mm)	170	170	170	195	220
R_2-R_1 (mm)	90	70	50	50	70

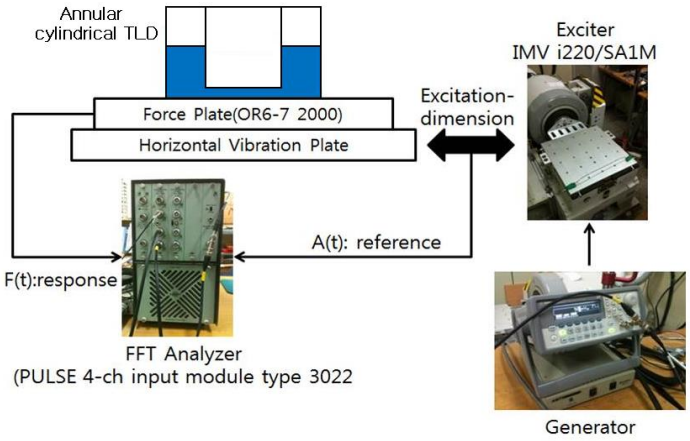

Fig. 4 Experiment apparatus

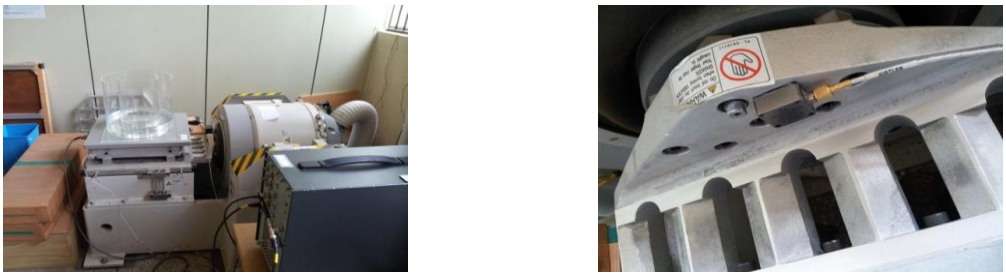

(a) (b)

Fig. 5 (a) Scene of actual sloshing experiment, (b)

Fig. 4 represents an experiment apparatus composed of generator, exciter, FFT analyzer and annular cylindrical TLD, where a random signal white noise at 0~25Hz is delivered to a shaker so as to excite a horizontal vibration table. Fig. 5 shows a scene of actual sloshing experiment, in which acceleration as an input signal was measured by attaching an accelerometer to the shaker table connector as shown in Fig. 5(b). A strain gage-type force plate was installed on the horizontal vibration table and the damper was put on it. As output signal, the force plate measures the transmission force of the floor which is caused by interior liquid sloshing in the annular cylindrical TLD. The apparent mass $H(\omega)$, a kind of frequency response function (FRF), defined as the output (force exerted on the vibration plate) per unit input (acceleration of the vibration plate)

$$H(\omega)=\frac{output}{input}=\frac{force exerted\ on\ the\ vibration\ plate}{acceleration\ of\ the\ vibration\ plate} \tag{4}$$

and its theoretical derivation is given in Appendix.

Table 2 Setting of FFT analyzer

Span	Lines	Resolution	Overlap	Average
12.5 Hz	800	0.015625 Hz	75%	20

Table 3 Specifications of equipments

Accelerometer (Kistler 8310B10)	Acceleration range	Sensitivity, 5%	Resolution (threshold)	Frequency Response, 5%	Noise type ($0 \sim 100 Hz$)
	10 g	197 mV/g	2,830 μg	0~180 Hz	2,000 μg_{rms}
Force plate (OR6-7 2000)	Capacity	Sensitivity	Excitation	Hysteresis	Natural frequency
	4,450 N	0.34 mV/N	Max 10 V	0.2%	370 Hz
Exciter (i220/SA1M)	Frequency range		Maximum acceleration and payload		
	DC ~ 2,500 Hz		203 m/s^2, 200 kg		

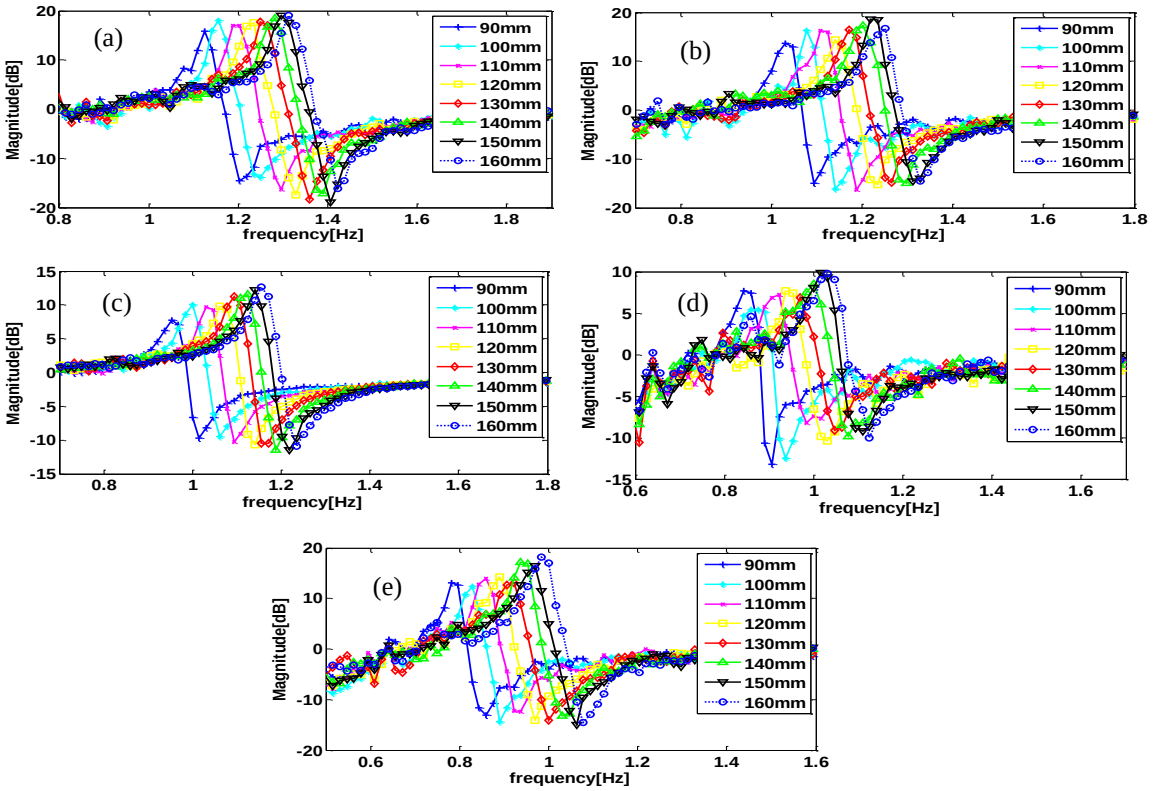

Fig. 6 Apparent masses of annular cylindrical TLD models near the first natural sloshing frequency: (a) model A, (b) model B, (c) model C, (d) model D, (e) model E

Setting of the FFT analyzer for the experiment is given in Table 2 and Table 3 represents the specifications of each component in the experiment apparatus. The experiments were repeatedly carried out by increasing the height of water in the annular cylindrical TLD from 90 to 160 mm with the interval of 10 mm.

Table 4 Fundamental natural sloshing frequencies of each model to the liquid fill height (unit: Hz)

Liquid fill height h_w (mm)	90	100	110	120	130	140	150	160
Model A	1.125	1.145	1.203	1.234	1.250	1.281	1.297	1.313
Model B	1.031	1.078	1.109	1.141	1.172	1.203	1.219	1.250
Model C	0.953	1.000	1.031	1.062	1.094	1.125	1.141	1.156
Model D	0.844	0.867	0.922	0.938	0.967	1.000	1.016	1.031
Model E	0.781	0.828	0.859	0.891	0.922	0.938	0.969	0.984

4. Experimental results

Fig. 6 represents the parametric characteristics of apparent mass of each model to the liquid fill height h_w near the first natural sloshing frequency, where the magnitude means the apparent mass. Please refer to Appendix on the fact that the apparent mass shows the peak value at the natural sloshing frequency. It is clearly observed that the first sloshing frequency is significantly affected by the liquid fill height as well as the radii of container, implying that the current annular cylindrical TLD could be tuned by controlling the liquid fill height. All the TLD models show the variations of apparent masss to the liquid fill height, which is consistent with the work by Min and Park (2009) who studied this tendency by calculating the transfer function of TLCD using the shaking table experiment.

It is found from Table 4 that the first natural sloshing frequency increases in proportion to the liquid fill height for all TLD models. Meanwhile, it shows the uniform increase with the inner radius of the container as well as the outer radius. It has been reported, according to Lamb (1932), that the fundamental resonant sloshing frequency of usual circular TLD is expressed by

$$f_r = \frac{1}{2\pi}\sqrt{\frac{1.841g}{R}\tanh\left(\frac{1.841h_w}{R}\right)} \tag{5}$$

Where, g is the acceleration of gravity, h_w the liquid fill height, and R is outer radius of circular damper. It can be found from Eq. (5) that frequency and radius of TLD are in the inverse relation, and the parametric experimental results given in Table 4 is consistent with Eq. (5) by letting R_1 of the annular cylindrical TLD as the characteristic radius.

The apparent masses of five TLD prototypes near the second natural sloshing frequency were also parametrically tested for eight different liquid fill heights, and the experimental results are represented in Fig. 7. Contrary to the previous results shown in Fig. 6, it is observed that the apparent masses near the second natural sloshing frequency are almost independent of the liquid fill height. Rather, they show the monotonic increase with the gap size $R_2 - R_1$ between the outer and inner radii of the acryl TLDs because the gap size is largest at model A and vice versa at models C and D, as given in Table 1. Meanwhile, from the comparison between two models C and D and between another two models B and E, it is observed that the apparent mass slightly increases with the outer radius R_2 when the gap size is equal. The difference in apparent masses between two different natural sloshing frequencies is caused because the second natural sloshing mode is different from the first natural sloshing mode. According to Faltinsen (2009) and Cho *et al*. (2000) who studied the natural sloshing behavior of liquid partially filled in annual circular tanks, the liquid free surface exhibits a seesaw-like fluctuation at the first natural sloshing frequency while it does a full sine wave-like fluctuation at the second natural sloshing frequency.

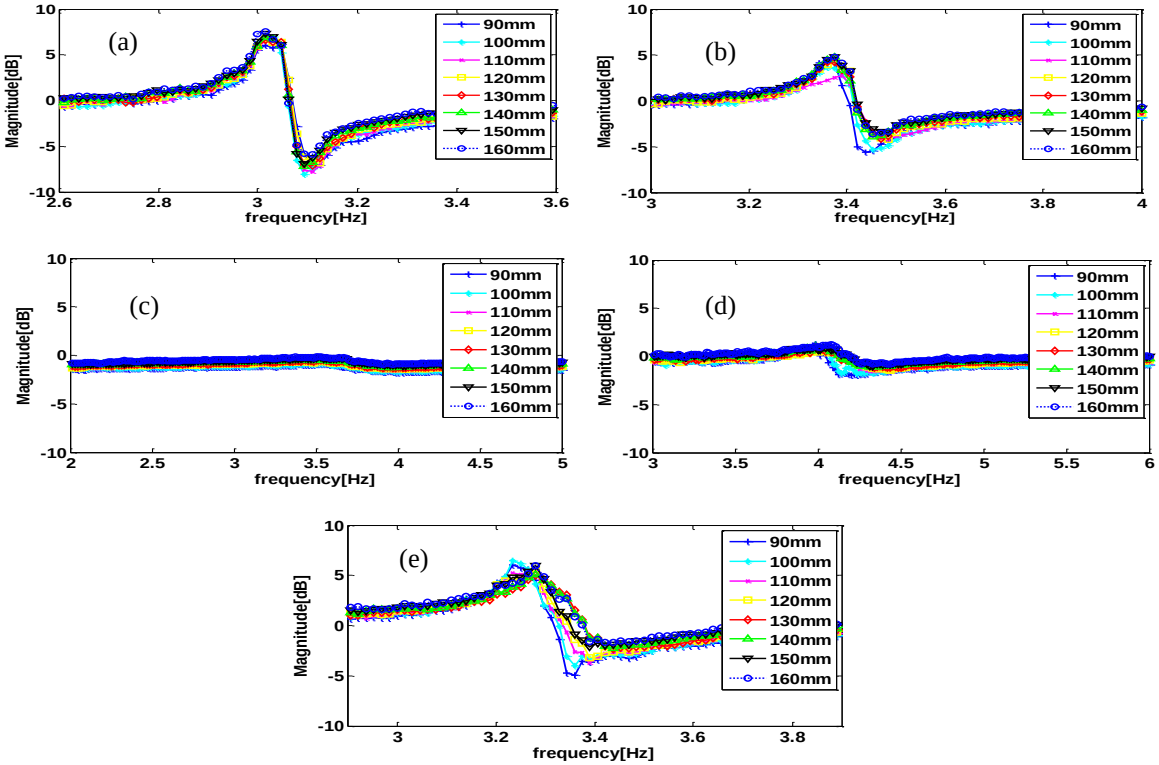

Fig. 7 Apparent masses of annular cylindrical TLD models near the second natural sloshing frequency: (a) model A, (b) model B, (c) model C, (d) model D, (e) model E

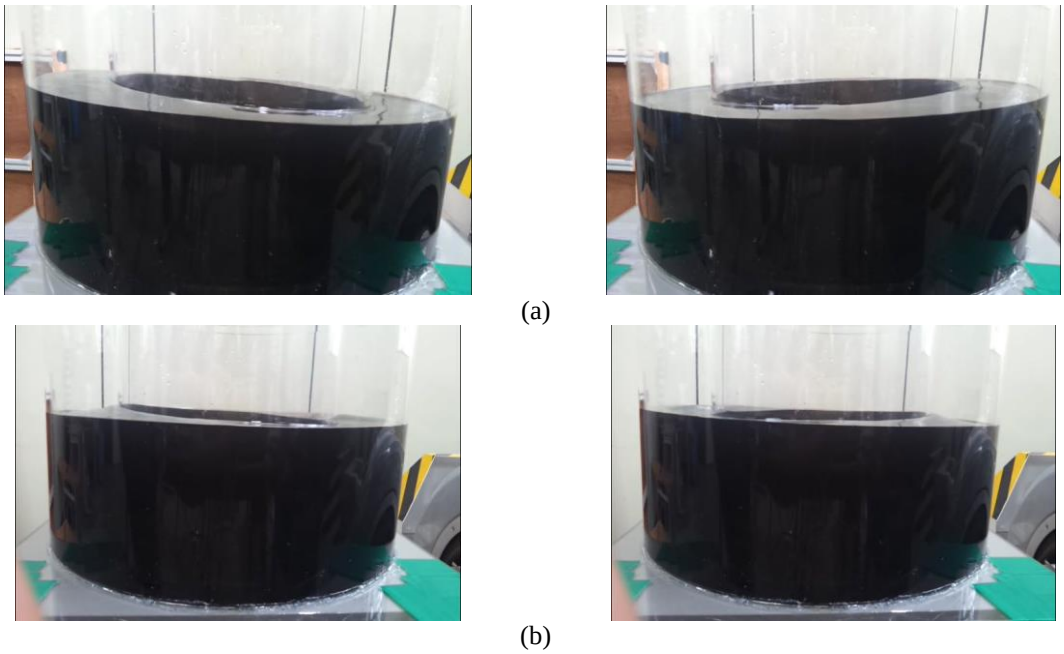

(a)

(b)

Fig. 8 Sloshing mode shapes: (a) first, (b) second

From this difference, the apparent mass near the first natural sloshing frequency becomes sensitive to the container radius and the liquid fill height while it at the second natural sloshing frequency does to the gap size.

Two lowest natural sloshing modes of water in the annular cylindrical TLD are represented in Fig. 8. As mentioned above, the first natural sloshing mode shows a seesaw-like sloped free surface motion. Meanwhile, the second sloshing mode shows a full sine wake-like free surface motion such that water on the left moves up while one on the right moves down. However, it is worth to mention that the damping performance of TLD, as a passive damping device, is dominated by the first natural sloshing.

5. Conclusions

In this paper, the natural sloshing frequencies of annular cylindrical TLD have been parametrically investigated by experiment. Five acryl prototypes of annular cylindrical TLD with different inner and outer radii were used, and eight cases of liquid fill height were examined for each TLD model. According to the parametric experiments, the following main observations were made:

• The first natural sloshing frequency increases in proportion to the liquid fill height for all TLD models, while it shows the uniform increase with the inner radius as well as the outer radius of container.

• The apparent mass near the first natural sloshing frequency becomes sensitive to the container radius and the liquid fill height.

But, the apparent masses near the second natural sloshing frequency are almost independent of the liquid fill height, rather they show the monotonic increase with the gap size of container.

Therefore, it has been confirmed that the annular cylindrical TLD could be used as an effective passive damping device for spar-type floating wind turbine, in aspects of the tuning possibility of first natural sloshing frequency as well as the easy installation, multi-directional damping performance and mass effectiveness.

Acknowledgements

This work was supported by the Human Resources Development of the Korea Institute of Energy Technology Evaluation and Planning (KETEP) grant funded by the Korea government Ministry of Knowledge Economy (No. 20114030200070).

References

Balendra, T., Wang, C.M. and Cheong, H.F. (1995), "Effectiveness of tuned liquid column dampers for vibration control of tower", *Engineering Structure*, **17**(9), 668-675.

Biran, A.B. (2003), *Ship Hydrostatics and Stability*, Butterworth-Heinemann, Singapore.

Cho, J.R., Lee, J.K. and Song, J.M. (2000), "Free vibration analysis of aboveround LNG-storage tanks by the finite element method", *KSME International Journal*, **14**(6), 633-644.

Cho, J.R. and Lee, S.Y. (2002), "Dynamic analysis of baffled fuel-storage tanks using the ALE finite element method", *International Journal for Numerical Methods in Fluids*, **41**(2), 185-208.

Cho, J.R. and Lee, H.W. (2004), "Numerical study on liquid sloshing in baffled tank by nonlinear finite element method", *Computer Methods in Applied Mechanics and Engineering*, **193**(23-26), 2581-2598.
Cho, J.R., Han, K.C., Hwang, S.W., Cho, C.S. and Lim, O.K. (2012), "Mobile harbor: structural dynamic response of RORI crane to wave-induced rolling excitation", *Structural Engineering Mechanics*, **43**(5), 679-690.
Colwell, S. and Basu, B. (2009), "Tuned liquid column dampers in offshore wind turbines for structural control", *Engineering Structures*, **31**, 358-368.
Dean, R.G. and Dalrymple, A.D., (1984), *Water Wave Mechanics for Engineers and Scientists*, 1st Edition, Prentice-Hall, New Jersey.
Faltinsen, O.M. (1990), *Sea Load on Ships and Offshore Structures*, University of Cambridge.
Faltinsen, O.M. and Timokha, A.N. (2009), *Sloshing*, Cambridge University Press.
Hansen, A.D. and Hansen, L.H. (2007) "Wind turbine concept market penetration over 10 years (1995-2004)", *Wind Energy*, **10**, 81-97.
Jin, Q., Li, X., Sun, N., Zhou, J. And Guan, J. (2007), "Experimental and numerical study on tuned liquid dampers for controlling earthquake response of jacket offshore platform", *Marine Structures*, **20**, 238-254.
Karimirad, M., Meissonnier, Q., Gao, Z. And Moan, T. (2011), "Hydroelastic code-to-code comparison for a tension leg spar-type floating wind turbine", *Marine Structures*, **24**, 412-435.
Lamb, H. (1932), *Hydrodynamics*, 6th Edition, Cambridge University Press.
Lee, H.H., Wong, S.H. and Lee, R.S. (2006), "Response mitigation on the offshore floating platform system with tuned liquid column damper", *Ocean Engineering*, **33**, 1118-1142.
Lefebvre, S. and Collu, M. (2012) "Preliminary design of a floating support structure for a 5MW offshore wind turbine", *Ocean Engineering*, **40**, 15-26.
Min, K.W. and Park, E.C. (2009), "Dynamic characteristics of tuned liquid column dampers using shaking table test", *The Korean Society for Noise and Vibration Engineering*, **19**(6), 620-627.
Miyata, T., Yamada, H. and Saito, Y. (1989), "Feasibility study of the sloshing damper system using rectangular containers", *Journal of Structural Engineering*, **35A**, 553-560.
Morsy, H. (2010), "A Numerical Study of the Performance of Tuned Liquid Dampers", MD Thesis, MaMaster University, Hamilton, Canada.
Yammamoto, K. and Kawahara, M. (1999), "Structural oscillation control using tuned liquid damper", *Computers and Structures*, **71**, 435-446.

Appendix: Theoretical derivation of apparent mass $H(\omega)$

The sloshing experiment apparatus shown in Fig. 4 which is composed of a horizontal vibration plate and an annular cylindrical TLD can be modeled as a two-DOF mass-spring system, as represented in Fig. A1. Where, M_1 indicates the equivalent mass of the vibration plate, m_2 and k_3 denote the equivalent mass and stiffness of the annular cylindrical TLD, respectively.

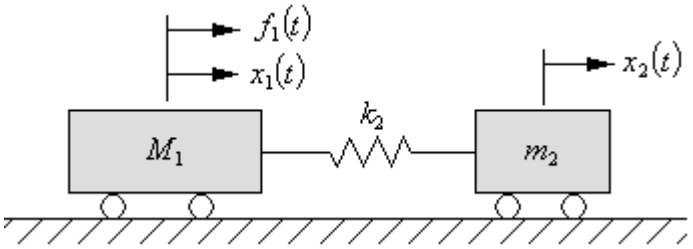

Fig. A1 A two-DOF dynamic model of the sloshing experiment apparatus

Letting $x_1(t)$ and $x_2(t)$ be the absolute horizontal dynamic motions of the vibration plate and the annular cylindrical TLD and $f_1(t)$ be the excitation force, then the equations of motion of the two-DOF dynamic model is expressed by

$$\begin{bmatrix} M_1 & 0 \\ 0 & m_2 \end{bmatrix} \begin{Bmatrix} \ddot{x}_1(t) \\ \ddot{x}_2(t) \end{Bmatrix} + \begin{bmatrix} k_2 & -k_2 \\ -k_2 & k_2 \end{bmatrix} \begin{Bmatrix} x_1(t) \\ x_2(t) \end{Bmatrix} = \begin{Bmatrix} f_1(t) \\ 0 \end{Bmatrix} \tag{A1}$$

For harmonic excitation force $f_1(t) = Fe^{iwt}$, the resulting two absolute dynamic motions are expressed by $x_1(t) = A_1e^{iwt}$ and $x_2(t) = A_2e^{iwt}$. Substituting these harmonic responses into Eq. (A1) ends up with

$$\begin{bmatrix} M_1 - \dfrac{1}{\omega^2}k_2 & \dfrac{1}{\omega^2}k_2 \\ \dfrac{1}{\omega^2}k_2 & m_2 - \dfrac{1}{\omega^2}k_2 \end{bmatrix} \begin{Bmatrix} A_1 \\ A_2 \end{Bmatrix} = \begin{Bmatrix} F \\ 0 \end{Bmatrix} \tag{A2}$$

Solving the simultaneous equations leads to the amplitude A_1 given by

$$A_1 = \frac{\left(m_2 - \dfrac{k_2}{\omega^2}\right)F}{\left(M_1 - \dfrac{k_2}{\omega^2}\right)\left(m_2 - \dfrac{k_2}{\omega^2}\right) - \dfrac{1}{\omega^4}k_2^2} \tag{A3}$$

Finally, according to the definition given in Eq. (4), the apparent mass $H(\omega)$ of the annular cylindrical TLD is calculated by

$$H(\omega) = \frac{F}{A_1} = \frac{\left(\omega^2 M_1 - k_2\right)\left(\omega^2 m_2 - k_2\right) - k_2^2}{\omega^2\left(\omega^2 m_2 - k_2\right)} \tag{A4}$$

Therefore, $H(\omega)$ has the peak value at the natural sloshing frequency of $\omega_r = \sqrt{k_2 / m_2}\ (rad/s)$

(or, $f_r = \omega_r / 2\pi\,(Hz)$), whereas the anti-resonance of apparent mass occurs at the frequencies which make the numerator of Eq. (A4) zero. It is found that both the resonance and anti-resonance of apparent mass are dependent of the equivalent mass and stiffness of TLD as well as the equivalent mass of the vibration plate.